Thermal and Flammability Properties of a Silica–Poly(methylmethacrylate) Nanocomposite

Takashi Kashiwagi,[1,*] Alexander B. Morgan,[1,†] Joseph M. Antonucci,[2] Mark R. VanLandingham,[3] Richard H. Harris, Jr.,[1] Walid H. Awad,[1,†] John R. Shields[1]

[1]*Fire Science Division, Building and Fire Research Laboratory, National Institute of Standards and Technology, Gaithersburg, Maryland 20899*
[2]*Polymer Division, Materials Science and Engineering Laboratory, National Institute of Standards and Technology, Gaithersburg, Maryland 20899*
[3]*Building Materials Division, Building and Fire Research Laboratory, National Institute of Standards and Technology, Gaithersburg, Maryland 20899*

Received 3 June 2002; accepted 26 October 2002

ABSTRACT: PMMA, poly(metheylmethacrylate), nanocomposites were made by *in situ* radical polymerization of MMA, methylmethacrylate, with colloidal silica (ca. 12 nm) to study the effects of nanoscale silica particles on the physical properties and flammability properties of PMMA. Transparent samples resulted and the dispersity of the particles was examined by transmission electron microscopy and atomic force microscopy. The addition of nanosilica particles (13% by mass) did not significantly change the thermal stability, but it made a small improvement in modulus, and it reduced the peak heat release rate roughly 50%. Last, the flame-retardant mechanism provided by the addition of nanosilica particles in PMMA is discussed. © 2003 Wiley Periodicals, Inc. J Appl Polym Sci 89: 2072–2078, 2003

Key words: nanocomposite; silica; poly(metheylmethacrylate); flammability

INTRODUCTION

The properties of a composite material depend not only upon the properties of the individual component phases (matrix, filler, interphase), but also upon their interaction. The composite's phase morphology can have significant effects on properties and this morphology significantly depends on interphase interaction, if the area of the interface between the two components becomes significantly large.[1,2] One such application, an improvement in flammability properties of polymers using the unique interface that can develop with layered silicates, has been demonstrated for clay nanocomposites of various resins.[3–8] The advantage of the use of layered silicates as flame-retardant additives is that they not only improve the flammability properties but also improve physical properties of the composite relative to the polymer matrix.[9–13] In contrast, conventional flame-retardant additives, such as brominated compounds and hydrates, improve the flammability of polymers but tend to reduce many of their physical properties. Although the flame-retardant mechanism of polymer–clay nanocomposites has not been well resolved, several hypotheses have been proposed. They are the formation of char that serves as a barrier to degradation products and as a heat insulation layer,[6,8] a catalytic charring action of the strongly acidic proton sites created in the silicate by thermal degradation of the organic modifier,[7] and radical trapping by the presence of paramagnetic iron in the clay matrix.[14]

Nanoscale silica particles also can have a large interfacial area as long as the diameter of the particles is in the range of nanometers and they are well dispersed in the polymer. Although they do not have the narrow gallery structure of a layered clay (severely constraining the mobility of polymer chains in these galleries), the improvement in physical properties[15–18] and also some improvement in thermal stability[19] by the addition of nanoscale silica particles to polymers were reported. Although the addition of mesoscale silica particles to various polymers significantly reduced heat release rate of the polymers,[20,21] there are no previous studies on the flame-retardant effectiveness of the nanosilica addition. It was reported that polymers filled with nanoscale size silica particles exhibit a second, apparent glass transition at a much higher temperature than that of the polymer resins.[22] This phenomenon was attributed to the formation of tightly bound and loosely bond polymer chains around the particles, which might improve the thermal stability of the polymer and subsequently flam-

Correspondence to: T. Kashiwagi (Kashiwaga@nist.gov).
* Guest Researcher.
† Currently at Dow Chemical Co.

Journal of Applied Polymer Science, Vol. 89, 2072–2078 (2003)
Published by Wiley Periodicals, Inc.

mability properties. Thus, the present study is intended to explore the applicability of nanoscale silica particles to poly(metheylmethacrylate), PMMA, as a flame-retardant additive to improve simultaneously the flammability properties and the physical properties of this polymer.

EXPERIMENTAL

Materials

In a round-bottomed flask, 14 g of MEK-ST [30% by weight colloidal silica in methyl ethyl ketone (MEK), Nissan Chemical Industries, Ltd., Houston, TX[‡]] and ca. 40 mL of methyl methacrylate (MMA, Sigma–Aldrich, Milwaukee, WI) were mixed. The mixture was placed on a rotary evaporator and MEK was removed with constant stirring at 62°C and a pressure of 23.4 kPa by removing 20 ± 5 g of the MMA and MEK mixture. Then MMA was added to the flask to bring the weight of MMA to 37.8 g. The flask was stoppered and mixed for 900 s in a sonic bath. Benzoyl peroxide (1.7% based on the MMA mass) was added to the flask with constant stirring for 900 s. The clear mixture was transferred to a stainless steel beaker and covered tightly with heavy duty aluminum foil. Free radical polymerization was achieved in a convection oven at 45°C for 48 h. The sample was then transferred to a vacuum oven at 80°C and 23.4 kPa for 72 h. This procedure was designed to prepare a 42 g disk with a nominal diameter of 7.6 cm and a thickness of 0.8 cm. The actual disks are ca. 8 cm diameter and 0.6 cm thick. Exactly the same procedure was used to make PMMA samples using MEK without any silica particles. The number averaged molecular weight of this PMMA, measured by a size-exclusion chromatography, was 147,000 ± 1000[§] and that of the PMMA of the nanosilica composite was 183,000 ± 8000. The polydispersities of both samples were 1.9 ± 0.1. Actual content of silica particles in the PMMA–SiO_2 sample was determined by pyrolyzing the sample in air at 900°C in a muffle furnace. By weighing the white powdery residue, a value of 13 ± 1% by mass was found. This higher value of silica content above the intended 10% mass fraction was caused by the loss of some MMA during the removal of MEK from the MMA and MEK mixture.

[‡] Certain commercial equipment, instruments, materials, services, or companies are identified in this article in order to specify adequately the experimental procedure. This in no way implies endorsement or recommendation by NIST.

[§] According to ISO 31-8, the term "molecular weight" has been replaced with "relative molecular mass," symbol M_r. The conventional notation, rather than the ISO notation, has been employed for this publication.

Instrumentation

Bright field TEM images of the PMMA/nanosilica sample were obtained at 120 kV, under low-dose conditions, with a Phillips 400T electron microscope. The sample was ultramicrotomed with a diamond knife at 23°C to give ~70 nm thick sections. The sections were transferred from water to carbon-coated (type B) Cu grids of 200 mesh.

Atomic force microscopy (AFM) was performed using a Digital Instruments Dimension 3100 AFM with a Nanoscope 3a controller. Tapping mode imaging was performed using a single-beam silicon cantilever probe with a nominal resonance frequency around 300 kHz and a nominal tip radius of 5–10 nm. Topographic and phase contrast images were collected using a root mean square (RMS) free amplitude of (65 ± 5) nm and a set-point amplitude to RMS amplitude ratio of approximately 0.5. Samples were prepared for AFM investigation by first sectioning a molded plaque with a band saw and then mounting the sectioned sample in epoxy potting compound. The epoxy was left to cure at room temperature for 24 h. The cross-sectioned sample in epoxy was then polished first using a series of silicon carbide polishing papers followed by a series of diamond pastes of decreasing grit size, the last of which was a 0.25 μm paste. Finally, the polished surface was cleaned with soap, rinsed with distilled water and methanol, and dried with hot air.

Thermal gravimetric analysis (TGA) data were collected from 30 to 800°C at 10 °C/min under nitrogen using a TA Instruments, SDT 2960.

Dynamic mechanical analysis (DMA) was performed using a Rheometrics Solid Analyzer (RSA) II. Samples having approximate dimensions of 52 mm in length by 12 mm in width by 3.5 mm in thickness were tested in flexure at a frequency of 10 Hz and a dynamic strain of 0.05%. These samples were prepared by cutting a molded plaque using a band saw. Experiments were conducted from 30 to 135°C using variable temperature increments and dwell times of at least 4 min, i.e., after each temperature increment, the new temperature was held constant for at least 4 min prior to recording the measured material response. Storage modulus, E', loss modulus, E'', and loss tangent, tan (δ) were recorded as a function of temperature. The glass transition temperature, T_g, was taken to be the peak in the tan(δ) curve.

Evaluation of flammability properties was achieved using the Cone calorimeter, which was designed and built at NIST (ASTM E 1354-92). Aluminum foil was wrapped around the sample except on the irradiated surface as a sample container instead of the standard, heavy metal container. The tests were performed at an incident radiant flux of 40 kW/m^2 in air. Heat release rate and mass loss rate are reproducible to within ±10%. Another device, a radiative gasification instrument similar to the Cone calorimeter, was used to

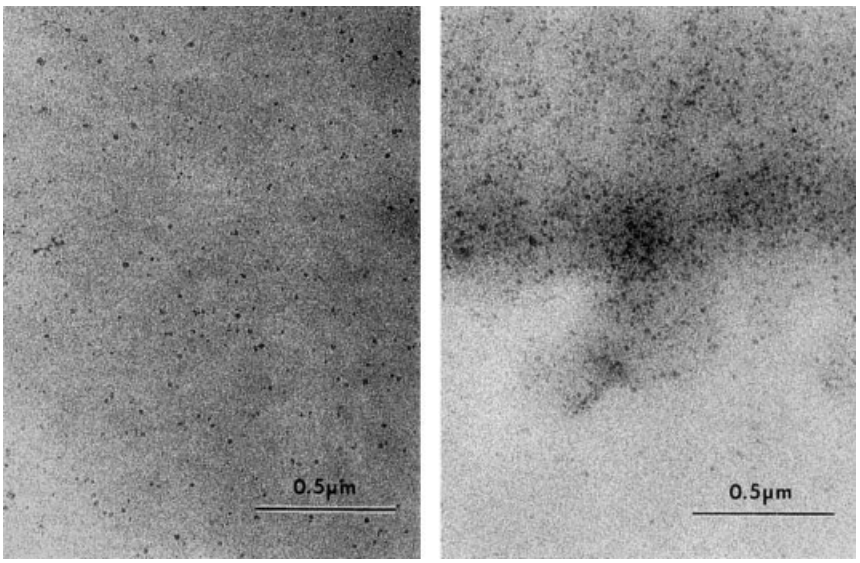

Figure 1 TEM images of PMMA/nanosilica sample at two different locations with low magnification.

observe the gasification behavior and to measure mass loss rate of the sample in a nitrogen atmosphere (no burning) at 40 kW/m^2. A more detailed discussion of the device is given in our previous study.[23] The unique advantages of this device are twofold: the first is that the results obtained from it are based only on the condensed phase processes due to the absence of any gas phase oxidation reactions; the second is it enables visual observation of gasfication phenomena under a heat flux similar to that of a fire without any interference from a flame.

RESULTS

Characterization of nanocomposites by TEM and AFM

All polymerized samples were clear and transparent both with and without the nanosilica particles, but all had a faint yellow color that might be caused by the use of benzoyl peroxide as the initiator. Although the transparency of the samples with nanosilica particles suggests reasonably good dispersion of the particles in the PMMA, TEM and AFM images were taken to examine dispersion at a particle scale. TEM analysis of the PMMA/nanosilica sample at low magnification shows well dispersed areas and also areas of greater silica particle concentration without clustering, as shown in Figure 1. The TEM image in Figure 2 at high magnification shows well-dispersed 10–30 nm silica spheres.

Tapping mode AFM images were taken of a polished section of a molded PMMA/nanosilica sample. Topographic and phase contrast images are shown in Figure 3. Because this cross-sectional sample was polished, the overall height changes over the 1×1 μm area are small, with a peak-to-valley roughness of less than 20 nm. The polishing direction is also evident in the topographic image. The phase contrast in the right images is likely caused by repulsive tip–sample interactions with the nanosilica, resulting in a positive phase and brighter areas or features, and an attractive tip–sample interaction with the PMMA, resulting in a negative phase and darker areas. Because height changes not related to the presence of nanosilica particles occur, the nanosilica particles are easier to discern in the phase contrast image compared to the topographic image. In the phase image, a large number of what appear to be single nanosilica particles is observed. The corresponding particle sizes range from 12 to 30 nm, which compares to a nominal particle size of 12 nm. However, interaction of the tip with features

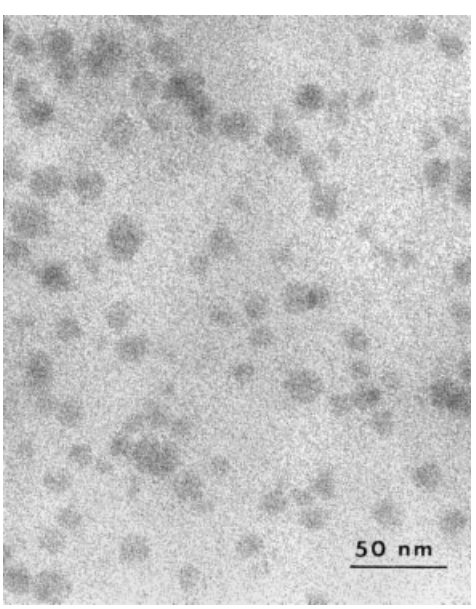

Figure 2 TEM image of PMMA/nanosilica sample with high magnification.

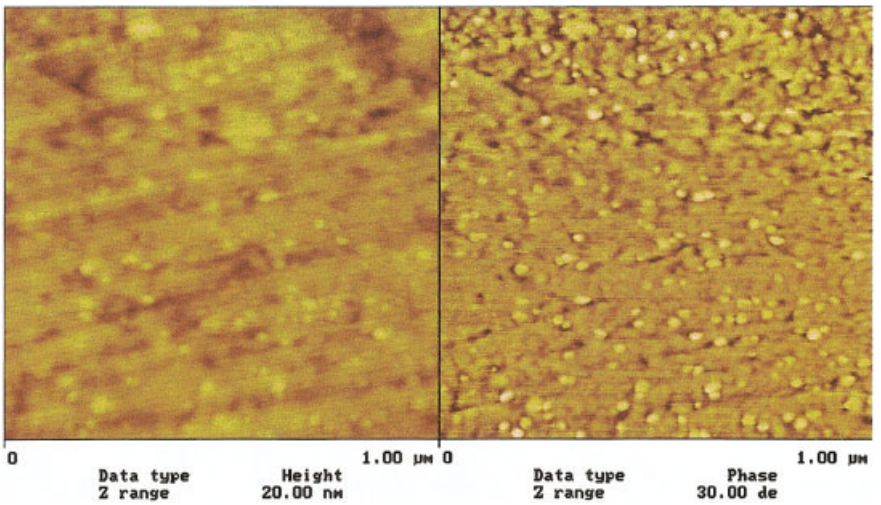

Figure 3 Tapping mode AFM images of a PMMA/nanosilica sample. The left image is the height or topographic image, while the right image is the phase contrast image. The color scales from black to white represent a height difference of 20 nm for the left image and a phase difference of 30° for the right image.

that are similar in size to the tip often results in an apparent broadening of the features. In this case, more interaction with the tip, and hence a larger broadening, will result for a nanosilica particle that is elevated topographically relative to the PMMA matrix vs a particle that is submerged in the PMMA. Thus, the apparent particle size distribution is likely related to different amounts of this broadening effect rather than a real distribution of particle sizes. Note, however, that the AFM images are of the cross-sectional sample's surface and the bright phase contrast indicates lateral positions of nanosilica at or very near the surface. Further, only a few areas of this sample were imaged. Thus, conclusions regarding dispersion based on this limited study are difficult. However, the observation of single nanoparticles in the AFM images indicates that relatively good dispersion was achieved and this finding correlates with the results of TEM.

TGA characterization of thermal stability

Normalized sample mass loss rate and its derivative with respect to temperature of the PMMA sample and the PMMA/nanosilica sample are plotted in Figure 4. It is known that radically polymerized PMMA starts to degrade by initiation at the head-to-head linkages (at around 160°C), initiation at the unsaturated ends (at around 270 °C), and random initiation along the polymer backbone (at around 360°C).[24] Generally, the contribution to sample mass loss from initiation at the head-to-head linkages is relatively small. However, initiation from the unsaturated ends becomes more significant with a decrease in relative molecular mass due to an increase in the number of unsaturated ends initially present. The mass loss rate results shown in Figure 4 correspond to the three types of initiation; the addition of nanosilica particles slightly reduced the thermal stability of the nanocomposite sample at low temperatures and slightly delayed random initiation along the polymer backbone. However, it appears that overall PMMA degradation mechanism was not significantly modified by the addition of nanosilica particles.

Mechanical characterization

DMA was performed on two samples each of PMMA and PMMA/nanosilica. Representative results are shown for the two sets of samples in Figures 5(a) and 5(b), respectively. In these figures, storage modulus, E', loss modulus, E'', and loss tangent, tan(δ), are plotted as a function of temperature. A relatively small increase in E' (at 30°C) was observed with the addition of the nanosilica from (3.1 ± 0.1) GPa for the PMMA to (3.7 ± 0.1) GPa for PMMA/nanosilica. A slight decrease in glass transition temperature was observed with nanosilica addition from (105 ± 2)°C for PMMA

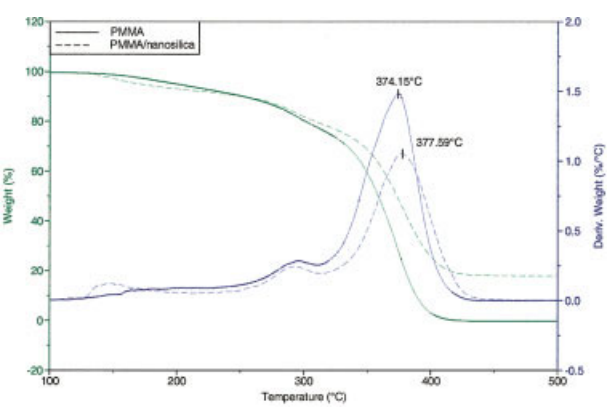

Figure 4 Comparison of TGA and DTG curves of PMMA and PMMA–silica samples.in nitrogen at 10°C/min.

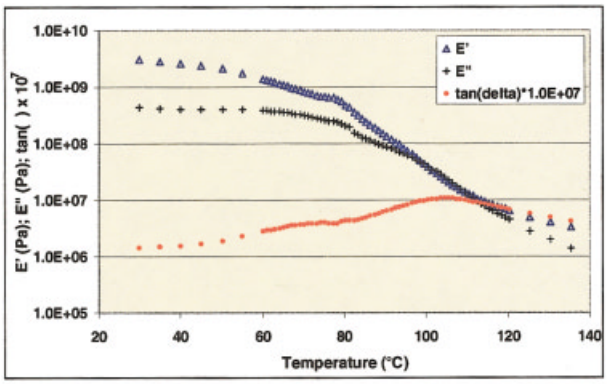

(a)

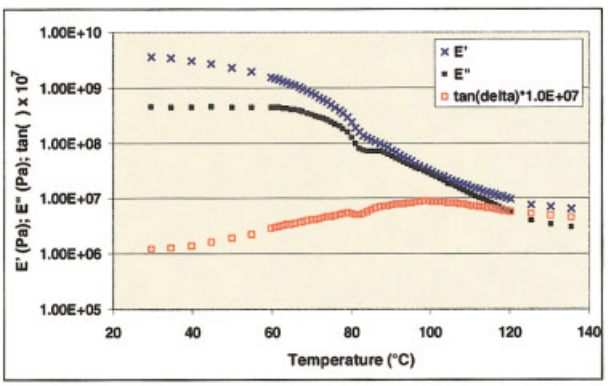

(b)

Figure 5 DMA results, plotted as E', E'', and tan(δ) as a function of temperature, are shown for (a) PMMA and (b) PMMA with 13% nanosilica by mass.

to (100 ± 2)°C for PMMA/nanosilica (this reduction is probably due to residual solvent in the sample as discussed later), and a greater enhancement in both moduli was observed above this temperature. For both sets of samples, changes in the slopes of E' and E'' and a small peak in tan(δ) were observed around 80°C. These occurrences might have been caused by auto-tension problems with the RSA II but might also be a result of the presence of residual MEK, which has a boiling point around 80°C. These effects appear to have been more dramatic for the PMMA/nanosilica than the PMMA, perhaps suggesting a higher amount of MEK left in these samples.

Gasification characterization

PMMA

Observation of the sequence of events in the gasification of the pure PMMA sample at a radiant flux of 40 kW/m^2 first revealed the appearance of small bubbles bursting at the sample surface around 15 s after the start of irradiation, followed by a rapid increase in the number of bubbles bursting so that they covered the entire sample surface after about 30 s. Around 120 s, the sample surface acquired the appearance of a fluid with larger bursting bubbles and with slight swelling as shown in Figure 6(A1). More vigorous bubbling appeared for times greater than 120 s and the sample became less viscous (more fluid in appearance). After 240 s, the surface was covered by large bursting bubbles and vigorous bubbling with a very fluid sample continued as shown in Figure 6(A2). At the end of the test, no significant amount of residue was left except a thin, black coating on the container surface.

PMMA/nanosilica nanocomposite

The gasification behavior of the PMMA/nanosilica sample was quite different from that of the above PMMA sample. Many small, bubbles were observed initially, but at about 60 s many white islands appeared on the sample surface with vigorous bursting of small bubbles around the islands. Around 120 s, the islands became darker and irregular as shown in Figure 6(B1). It appeared that the islands were made of coarse, granular particles. The coverage of the sample surface by the islands continued to increase and a random motion of granular particles on the sample surface was often observed. At about 300s, the sample surface was completely covered by coarse, granular particles as shown in Figure 6(B3). Also, the sample surface was slowly receding. At the end of the test, a dark, coarse powdery layer was left in the sample container. The fluid behavior observed for the PMMA sample was not seen for this sample. The mass of the residue was almost the same as that of the initial weight of nanosilica and the thickness of the residual layer at the end of the test was roughly half of the initial sample thickness. The observed gasification behavior of this sample is very similar to that of the low molecular weight PMMA/silica gel sample in our previous study.[21]

The calculated mass loss rates from the measured sample masses of PMMA and PMMA/nanosilica samples are plotted in Figure 7. The peak mass loss rate of the PMMA/nanosilica is roughly 40% less than that of PMMA. However, the mass loss rate up to 50 s and the total sample mass loss (integrated values of the mass loss curve) are about the same for both samples. These trends are very similar to those of the low molecular weight PMMA/silica gel sample.[21]

Heat release rate characterization

The heat release rates of the PMMA and the PMMA/nanosilica sample are shown in Figure 8. The addition of the nanosilica reduced the peak heat release rate of the PMMA sample to roughly 50% of the pure PMMA value, but ignition delay time and the total heat release (integrated values of the heat release rate curve) are about the same for both samples. The trends of the measured mass loss rate (burning rate) curves (not shown) are very close to those of the heat release rate curves and thus the calculated specific heat of com-

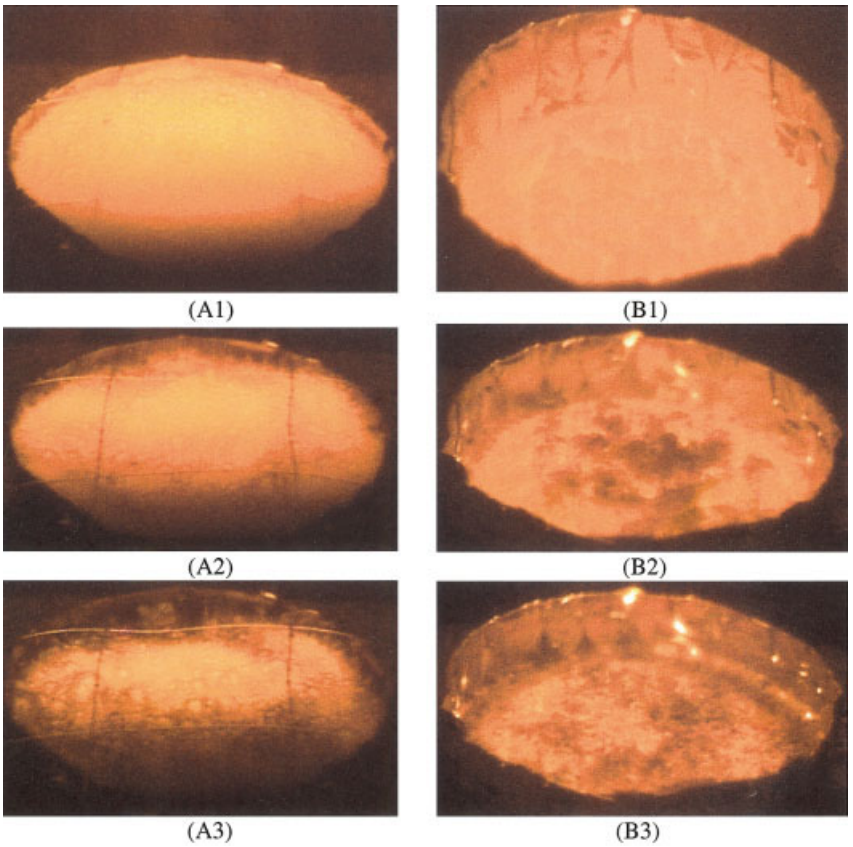

Figure 6 Selected sequence of video images of gasification phenomena of PMMA and PMMA/nanosilica samples in N_2 at 40 kW/m^2. A column: PMMA at 120 s (A1), 240 s (A2), and 300 s (A3); B column: PMMA/nanosilica at 120 s (B1), 240 s (B2), and 300 s (B3). The container of the PMMA sample was held by four small wires to avoid its movement.

bustion (measured heat release rate divided by measured mass loss rate) is 24 ± 2 MJ/kg for both types of sample. Furthermore, the trends of the heat release rate curves are very similar to those of the mass loss rate in nitrogen, as shown in Figure 7. The PMMA/nanosilica sample residue after Cone calorimeter tests was a gray layer consisting of coarse, granular powder accumulated at the bottom of the sample container.

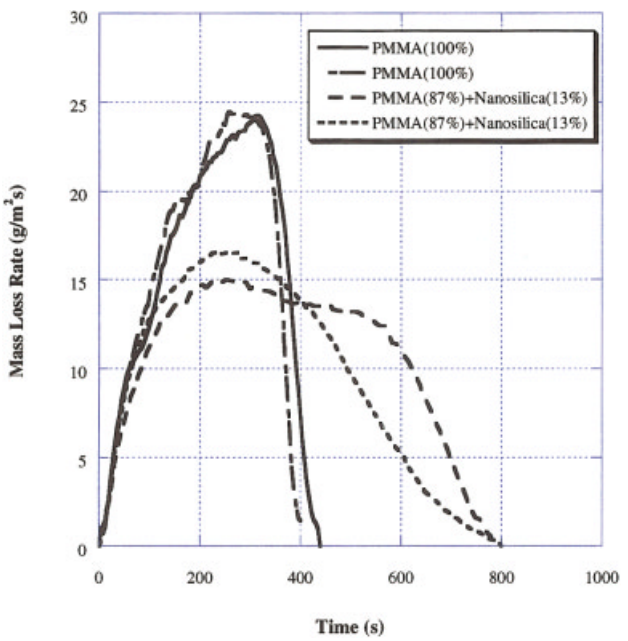

Figure 7 Effects of nanosilica addition on mass loss rate of PMMA at 40 kW/m^2 in nitrogen.

DISCUSSION

The unchanged specific heat of combustion and the similarity of the heat release rate curve to the mass loss rate curve in nitrogen for both the pure PMMA sample and the PMMA/nanosilica sample suggest that the reduction in heat release rate by the addition of nanosilica is mainly caused by the chemical and physical processes in the condensed phase rather than in the gas phase. It has been found that two important physical processes in the condensed phase are required to reduce significantly heat release rate by the addition of micron scale fused silica and silica gel. They are the accumulation of the added silica on the burning sample surface and complete coverage of the sample surface by the silica.[20,21] It appears that the required processes were achieved most effectively by the *in situ* formation of a silica network reinforced by char to form a protective layer as a heat insulation and a barrier of evolved degradation products.[21] The flame-

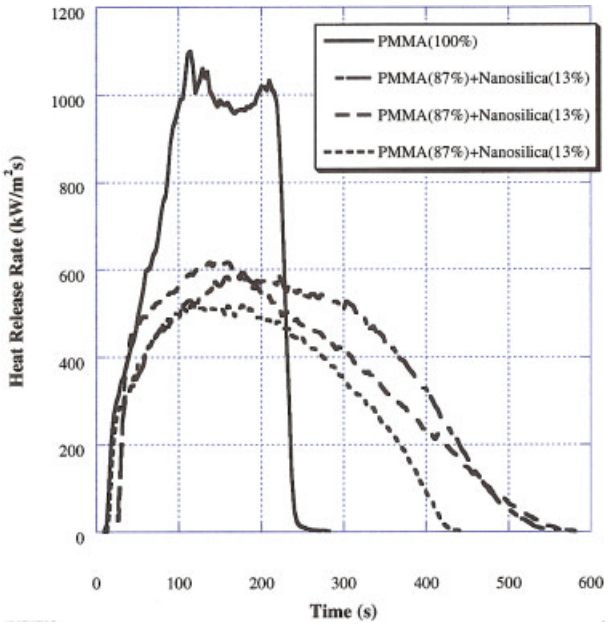

Figure 8 Effects of nanosilica addition on heat release rate of PMMA at 40 kW/m^2. The dashed lines were the results of three replica of nanocomposites made at three different times.

retardant effectiveness of the addition of nanosilica particles (by 13% mass) to PMMA is adequate, but not as good as that of the addition of silica gel to PMMA (60–70% reduction in peak heat release rate). The observations of the gasification of the PMMA/nanosilica indicate the fact that the nanosilica particles tend to accumulate and coagulate near the sample surface, forming loose, granular particles instead of a tight continuous silica network. Since the PMMA/nanosilica sample surface was covered by loose granular particles, part of the sample surface was still exposed to the external radiation through the granular particle layer and also the barrier performance of the layer to contain the degradation products of PMMA was not effective. Therefore, the addition of nanoscale silica particles to PMMA satisfied one of the two requirements but not both requirements. One possible approach to forming *in situ* silica network during gasification could be to enhance the formation of crosslinks among the particles by appropriate surface treatments of nanosilica particles.

CONCLUSION

Transparent PMMA nanocomposites were successfully made by *in situ* radical polymerization of MMA with colloidal silica particles having an average diameter of 12 nm. TEM and AFM analyses of the nanocomposites indicate well-dispersed areas and areas of greater silica particle concentration without clustering. The addition of nanosilica particles (13% by mass) did not significantly change the thermal stability—it made a small improvement in modulus, and it reduced the peak heat release rate by roughly 50%. The flame-retardant mechanism of the addition of the nanosilica particles to PMMA is inferred to be the coagulation of the particles and the accumulation of loose, granular particles near the sample surface to form a protective layer as a heat insulation and a barrier for evolved degradation products. Since the PMMA/nanosilica sample surface was covered by loose granular particles, part of the sample surface was still exposed to the external radiation through the granular particle layer. Therefore, flame-retardant effectiveness of the addition of the nanosilica particles in PMMA is not as good as the addition of silica gel in PMMA, which forms an *in situ* silica network to cover the entire sample surface. We note that better flame retardancy might be achieved by surface treating the silica particle to enhance the formation of the silica network.

References

1. Novak, B. M. Adv Mater 1993, 5, 422–433.
2. Alexandre, M.; Dubois, P. Mater Sci Eng 2000, R28, 1.
3. Giannelis, E. Adv Mater 1996, 8, 29–35.
4. Gilman, J. W.; Kashiwagi, T. SAMPE J 1997, 33, 40–46.
5. Gilman, J. W. Appl Clay Sci 1999, 15, 31–49.
6. Zhu, J.; Morgan, A. B.; Lamelas, J.; Wilkie, C. A. Chem Mater 2001, 13, 3774–3780.
7. Zanetti, M.; Camino, G.; Mulhaupt, R. Polym Degrad Stability 2001, 74, 413–417.
8. Gilman, J. W.; Jackson, C. L.; Morgan, A. B.; Harris, R., Jr.; Manias, E.; Giannelis, E. P.; Wuthernow, M.; Hilton, D.; Phillips, S. H. Chem Mater 2000, 12, 1866–1873.
9. Kojima, Y.; Usuki, A.; Kawasumi, M.; Okada, A.; Fukushima, Y.; Karauchi, T.; Kamigaito, O. J Mater Res 1993, 8, 1185–1189.
10. Kawasumi, M.; Hasegawa, N.; Kato, M.; Usuki, A.; Okada, A. Macromolecules 1997, 30, 6333–6338.
11. Wang, Z.; Pinnavaia, T. J. Chem Mater 1998, 10, 1820–1826.
12. Wang, Z.; Pinnavaia, T. J. Chem Mater 1998, 10, 3769–3771.
13. Manias, E.; Touny, A.; Wu, L.; Strawhecker, K.; Lu, B.; Chung, T. C. Chem Mater 2001, 13, 3516–3523.
14. Zhu, J.; Uhl, F. M.; Morgan, A. B.; Wilkie, C. A. Chem Mater 2001, 13, 4649–4654.
15. Landry, C. J. T.; Coltrain, B. K.; Landry, M. R.; Fitzgerald, J. J.; Long, V. K. Macromolecules 1993, 26, 3702–3712.
16. Hajji, P.; David, L.; Gerard, J. F.; Pascault, J. P.; Vigier, G. J Polym Sci. Part B 1999, 37, 3172–3187.
17. Ou, Y.; Yang, F.; Yu, Z.-Z. J Polym Sci, Part B 1998, 36, 789–795.
18. Reynaud, E.; Jouen, T.; Gauthier, C.; Vigier, G.; Varlet, J. Polymer 2001, 42, 8759–8768.
19. Hsiue, G.-H.; Kuo, W.-J.; Huang, Y.-P.; Jeng, R.-J. Polymer 2000, 41, 2813–2825.
20. Kashiwagi, T.; Gilman, J. W.; Butler, K. M.; Harris, R. H.; Shields, J. R. Fire Mater 2000, 24, 277–289.
21. Kashiwagi, T.; Shields, J. R.; Harris, R. H.; Davis, R. D. J Appl Polym Sci, in press.
22. Tsagaropoulos, G.; Eisenberg, A. Macromolecules 1995, 28, 396–398.
23. Austin, P. J.; Buch, R. R.; Kashiwagi, T. Fire Mater 1998, 22, 221–237.
24. Kashiwagi, T.; Inaba, A.; Brown, J. E.; Hatada, K.; Kitayama, T.; Masuda, E. Macromolecules, 1986, 19, 2160–2168.